

## Probable Maximum Precipitation Estimation Using Multifractals: Application in the Eastern United States

ELLEN M. DOUGLAS AND ANA P. BARROS

*Division of Engineering and Applied Sciences, Harvard University, Cambridge, Massachusetts*

(Manuscript received 8 August 2002, in final form 4 April 2003)

### ABSTRACT

Probable maximum precipitation (PMP) is the conceptual construct that defines the magnitude of extreme storms used in the design of dams and reservoirs. In this study, the value and utility of applying multifractal analysis techniques to systematically calculate physically meaningful estimates of maximum precipitation from observations in the eastern United States is assessed. The multifractal approach is advantageous because it provides a formal framework to infer the magnitude of extreme events independent of empirical adjustments, which is called the fractal maximum precipitation (FMP), as well as an objective estimate of the associated risk. Specifically, multifractal (multiscaling) behavior of maximum accumulated precipitation at daily (327 rain gauges) and monthly (1400 rain gauges) timescales, as well as maximum accumulated 6-hourly precipitable water fluxes for the period from 1950 to 1997 were characterized. Return periods for the 3-day FMP estimates in this study ranged from 5300 to 6200 yr. The multifractal parameters were used to infer the magnitude of extreme precipitation consistent with engineering design criterion (e.g., return periods of  $10^6$  yr), the design probable maximum precipitation (DPMP). The FMP and DPMP were compared against PMP estimates for small dams in Pennsylvania using the standard methodology in engineering practice (e.g., National Weather Service Hydrometeorological Reports 51 and 52). The FMP estimates were usually, but not always, found to be lower than the standard PMP (FMP/PMP ratios ranged from 0.5 to 1.0). Furthermore, a high degree of spatial variability in these ratios points to the importance of orographic effects locally, and the need for place-based FMP estimates. DMP/PMP ratios were usually greater than one (0.96 to 2.0), thus suggesting that DPMP estimates can provide a bound of known risk to the standard PMP.

### 1. Introduction

Determining the largest flood possible at a location is often necessary when designing high-hazard structures, such as flood control dams upstream of populated areas, for maximum reliability and safety. In the case where the risk of dam overtopping is deemed unacceptable, an estimate of the probable maximum precipitation (PMP) depth is used to determine the probable maximum flood (PMF) for that location. Use of the PMP to generate the PMF has become the standard for dam design in many parts of the world including the United States, China, India, and Australia (Svensson and Rakhecha 1998). The PMP is defined as the "theoretically greatest depth of precipitation for a given duration that is physically possible over a given size storm area at a particular geographical location at a certain time of the year" (Hansen et al. 1982). Prior to the 1950s, the concept was known as the maximum possible precipitation (MPP). The name was changed to the PMP reflecting the uncertainty surrounding any estimate of maximum

precipitation (Wang 1984). There is no known way to develop the PMP from first principles (NRC 1994) and proposed estimation methodologies have been the subject of much debate. By definition, the PMP is the estimated precipitation depth for a given duration, drainage area, and time of year for which there is virtually no risk of it being exceeded (Wang 1984). However, the fact that measured rainfall depths have exceeded PMP estimates in the past clearly indicates that the PMP approach "by no means implies zero risk in reality" (Koutsoyiannis 1999).

Graham (2000) criticized the use of current PMF standards for high-hazard dam spillway design. He noted that by using the PMF as a safety evaluation standard, most inspected nonfederal dams would have been deemed unsafe and, to adhere to current PMF design standards, the total retrofitting cost would amount to approximately \$75 billion. With this in mind, we investigate an alternative method for estimating maximum precipitation and associated risk for use in engineering design. We do so by first characterizing the scaling behavior of observed maximum precipitation depths and evaluating how these characteristics differ in both space and time. Recognizing that any estimates based on observations will be limited by the duration and quality

---

*Corresponding author address:* Dr. Ana P. Barros, Harvard University, Pierce Hall 118, 29 Oxford St., Cambridge, MA 02138.  
E-mail: barros@deas.harvard.edu

of the historical record, we propose to call this event fractal maximum precipitation (FMP). We then apply multifractal principles to extrapolate the magnitude of exceptional precipitation events for specified exceedance probabilities ( $Pe = 1 \cdot 10^{-6}$ ), the design probable maximum precipitation (DPMP).

#### a. Methods of PMP estimation

PMP estimation methods fall into the following general categories: the storm model approach; the maximization and transposition of individual observed storms; generalized (regionalized) methods; theoretical or empirical methods derived from maximum depth, duration, and area observations; and statistical methods. The storm model approach uses physical parameters, such as surface dewpoint, height of storm cell, and inflow and outflow, to represent the precipitation process (Collier and Hardaker 1996). Storm transposition involves translating observed storm characteristics from one or more gauged locations to the location where the PMP estimation is required (typically an ungauged location). Storm maximization consists of adjusting observed precipitation amounts upward to account for maximum atmospheric moisture convergence. Generalized PMP methods are often developed by maximizing and translating classes of storms over a broad region; storm classification in turn is based on the storm type, that is, convective or cyclonic (NWS 1988), and/or storm efficiency defined as the ratio of maximum observed rainfall to the amount of precipitable water in the storm column (Collier and Hardaker 1996). Factors that influence storm efficiency include atmospheric convergence; vertical velocity by frontal, convective, or topographically induced lifting; and the rate of water vapor condensation (Barros and Lettenmaier 1994; Svensson and Rakhecha 1998, and many others). Orographic effects are typically accounted for by adjusting PMP estimates derived for nonorographic regions.

Although the PMP has a theoretical exceedance probability of zero, meaning that it is so large that it will never be exceeded, this is not the case in reality. Consequently, a few studies have sought to assign a risk statement to PMP estimates. The National Research Council (NRC 1994) estimates the return period of the PMP in the United States as between  $10^5$  and  $10^9$  yr. Koutsoyiannis (1999) developed a rather straightforward method for assigning a return period to PMP values estimated using the frequency factor method (Hershfield 1961, 1965):

$$h_m = \bar{h}_n + k_m s_n, \quad (1)$$

where  $h_m$  is the maximum observed rainfall depth at the site of interest,  $\bar{h}_n$  and  $s_n$  are the mean and standard deviation of the annual maximum precipitation series for site  $m$ , and  $k_m$  is the frequency factor. Hershfield (1961) recommended  $k_m = 15$  for estimating the PMP, because it was the largest factor obtained from an anal-

ysis of 2645 stations (90% were from the United States). Later, Hershfield (1965) showed that  $k_m$  varied with rainfall duration and mean value and presented a nomograph for determining  $k_m$  for 5-min, 1-h, 6-h, and 24-h durations of mean annual maximum rainfall. Koutsoyiannis (1999) fit a generalized extreme value (GEV) distribution to the frequency factors computed from the 2645 record used by Hershfield and found that the largest factor ( $k_m = 15$ ) corresponds to a return period of about 60 000 yr, which falls at the low end of the NRC (1994) range. Foufoula-Georgiou (1989) investigated a storm transposition approach for assessing the frequency of extreme precipitation depths, but stressed the need for further research before applying the method to the PMP and PMF.

#### b. PMP estimation in the United States

The National Weather Service (NWS) has published and updated numerous hydrometeorological reports (HMRs) for estimating the PMP in different regions of the United States: HMR 59 (NWS 1999) for California, HMR 57 (NWS 1994) for the Pacific Northwest and Columbia Plateau regions, HMR 49 (NWS 1984) for the Southwest and basin and range regions, HMR 55A (NWS 1988) for the region east of the Continental Divide and west of the  $105^\circ$  meridian, and HMR 51 (NWS 1980a), HMR 52 (NWS 1982) and HMR 53 (NWS 1980b) for the United States east of the  $105^\circ$  meridian. HMR 52 outlines a procedure for preparing site-specific PMP estimates from the generalized storms presented in HMR 51. PMP estimation methods for smaller regions have also been published: HMR 54 for southeast Alaska (NWS 1983) and HMR 56 for Tennessee River drainages (NWS 1986). These reports can be found on the World Wide Web (<http://www.nws.noaa.gov/oh/hdsc/studies/pmp.html>). The NWS approach for estimating the PMP generally has three major components: moisture maximization, transposition to the location of interest, and envelopment of the maximized transposed depth-duration and depth-area amounts. Moisture maximization (adjusting record storm depths to account for what would have occurred with maximum atmospheric moisture) has traditionally been evaluated using the maximum persisting 12-h, 1000-hPa dewpoint, but in the most recent reports, moisture maximization based on sea surface temperatures was included. Storm transposition has been necessary in many cases due to the lack of local storm data, particularly in sparsely populated mountainous regions. Storm transposition for PMP estimation over the Appalachians and along the eastern seaboard required adjustments due to barrier effects and the fact that intensity of tropical storms drops off quickly with distance inland (NWS 1980a). Envelopment has been accomplished using smoothed isohyetal contours to generalize the maximized and transposed storm data, offering regionally consistent mapped values of PMP estimates. The shape of these isohyets

takes into account regional storm tracks and the regional distribution of maximum rainfall depths and atmospheric moisture.

The effect of complex terrain on moisture maximization and transposition complicates PMP estimation considerably and has been dealt with in different ways. In HMR 55A (NWS 1988), the region between the 103° and 105° meridians was first classified into orographic and nonorographic subregions delineated by an orographic separation line. The orographic region was further separated into “first upslopes” (areas of broader but more gradually increasing slope) and “secondary upslopes,” assuming that the first upslopes generally have the greatest effect on precipitation production. Other classifications within the orographic region were sheltered orographic subdivisions, relatively flat areas in which moisture transposition was affected by surrounding mountains, and ridges high enough to remove nearly all of the moisture from incoming air masses. Prior to analysis, storms were classified with respect to the type of terrain in which they occurred, and moisture maximization and storm transposition were adjusted accordingly. In California, mountains were found to sometimes shield an area from intense precipitation so both the enhancing and shielding effects of the terrain had to be accommodated by introducing a K factor, a percentage that either increases or decreases the nonorographically derived convergence precipitation.

In general, the PMP estimation method for areas east of the 105° meridian does not rigorously account for orographic effects. The exception to this is in HMR 56 (NWS 1986), where orographic effects in the Tennessee River valley were evaluated. Here, no clear spatial organization of events was evident and only slight increases in maximum precipitation amounts due to orographic effects were observed. HMR 51 (NWS 1980a) explicitly cautions potential users with regard to “deficient” PMP estimates over the Appalachian Mountains, an area that extends from northern Georgia into western Maine, and covers large sections of New England and the mid-Atlantic states. The need for a PMP method that accounts for orographic effects in this region was clearly illustrated by Barros and Kuligowski (1998) who found striking evidence of the linkages between the spatial organization of heavy precipitation and floods on the one hand, and landform in the Appalachian Mountains of Pennsylvania on the other. While the events are not necessarily PMP-magnitude events, Barros and Kuligowski illustrated how record floods in headwater catchments were associated with orographic enhancement of extreme precipitation events. This is consistent with the cautionary notes in HMR 51 referred above.

### c. Multifractal behavior of precipitation

Atmospheric processes consist of multiple highly nonlinear, complex dynamical processes (systems) that

interact with each other either continuously (as with radiation transfer) or intermittently (as with precipitation). Frisch and Parisi (1985) developed a multiplicative cascade model by noting the conditional self-similarity of fully developed turbulence (describing it as a “hierarchical embedding of bursts within bursts as one proceeds to smaller and smaller scales”) and developing a multifractal model consistent with a variety of observations in fully developed turbulence (Meneveau and Sreenivasan 1987). Lovejoy and Schertzer (1985, 1990) and Gupta and Waymire (1990) independently applied the multifractal (multiscaling) approach to describing the scaling behavior of rainfall and streamflow.

The multiplicative cascade model as applied to atmospheric phenomena can be understood by envisioning a large-scale eddy of characteristic length  $L$  being broken up into smaller subeddies whose length is equal to  $L/\lambda^i$ ,  $i = 1, \dots, n$ , where  $\lambda$  is the scale ratio. In the case of rainfall, Gupta and Waymire (1990) describe this phenomenon as clusters of high-intensity rainfall cells embedded within clusters of lower-intensity mesoscale cells, which are in turn embedded within a synoptic-scale lowest-intensity rainfall field (convection embedded in stratiform rainfall). Scale-invariant multiplicative cascades, such as described above, generically give rise to universal multifractals (Tessier et al. 1993). In fact, using satellite cloud images at both visible and infrared wavelengths over scales spanning 1–5000 km, Lovejoy et al. (2001) were able to show that variability at all observed scales and at all levels of intensity was very close to that predicted for a direct multiplicative scale-invariant cascade beginning at the planetary scale.

In the analysis of geophysical processes (i.e., turbulence, rainfall), we are almost always forced to analyze measurements that have been averaged over some small but finite sampling area with side  $\lambda > 0$  (i.e., the observing scale). The geophysical field in its original state is known as “bare,” while the measured field is known as “dressed.” Gupta and Waymire (1990) illustrated two important points with respect to the scaling properties of rainfall: 1) a spatially averaged (dressed) field scales with the same exponent as the original (bare) field, and 2) the scaling properties of rainfall fields, as well as other geophysical phenomena such as turbulent velocities and river flows, do not follow simple scaling behavior but are instead multiscaling (multifractal). Unlike simple scaling, in which the scaling exponent is a constant, the multifractal exponent is a function. Multifractal scaling properties can be described by the following two equations (Halsey et al. 1986; Meneveau and Sreenivasan 1987; Schertzer and Lovejoy 1987):

$$\varepsilon_\lambda \propto \lambda^\gamma \quad \text{for } \lambda > 1 \quad \text{and} \quad (2)$$

$$\Pr(\varepsilon_\lambda > \lambda^\gamma) \approx \lambda^{-c(\gamma)}, \quad (3)$$

where  $\Pr(\ )$  denotes probability;  $\varepsilon$  is the intensity (i.e.,

accumulated depth divided by duration) of a conservative field;  $\lambda$  is the scale ratio, which for time series is computed as the  $T/\tau$ , the length of the time series ( $T$ ) divided by the duration of interest ( $\tau$ );  $\varepsilon_\lambda$  is the conservative field at scale ratio  $\lambda$ ;  $\gamma$  is an order of singularity (maximum); and  $c(\gamma)$  is the convex functional scaling exponent known as the codimension. The convex nature of  $c(\gamma)$  implies a decrease in variability with respect to an increase in scale or vice versa (Gupta and Waymire 1990). There is a one-to-one correspondence between  $c(\gamma)$ , the scaling exponent in Eq. (3), and  $K(q)$ , the scaling exponent of the statistical moments of the field (Schertzer and Lovejoy 1992):

$$\langle \varepsilon_\lambda^q \rangle = \lambda^{K(q)} \quad \text{for } \lambda > 1. \quad (4)$$

Here  $q$  is the order of the statistical moment and  $\langle \rangle$  denotes the average of the field at scale  $\lambda$ . Olsson et al. (1993), Olsson (1995), and Tessier et al. (1996) utilized the relationship in Eq. (3) to evaluate the scaling properties of rainfall and river flows and cloud reflectance. Purdy et al. (2001) relied on the formalism of Eq. (4) to evaluate orographic effects during a single rainfall event along an orographic transect in the South Island of New Zealand. The double trace moment (DTM) method (Lavalée et al. 1991; Veneziano and Furcolo 1999), a relatively recent method for estimating multifractal parameters, is based on moment scaling. The DTM is discussed in more detail in section 2.

*d. Multifractals and the PMP*

A fundamental assumption underlying the concept of the PMP is that there exists some combination of physical conditions that would lead to a bounding precipitation event; in other words, for a given location there is a maximum amount of rainfall that can physically occur. The problems encountered when attempting to estimate extreme events (especially one that is considered to be an upper bound of the process) using conventional methods (i.e., frequency analysis or modeling) are twofold. First, the fitted probability distribution or the model that describes the majority of the historical time series (i.e., within two standard deviations of the mean) does not always capture the extremes. This reflects the fact that extreme events are often generated by unusual weather conditions instead of the climatology. There are also far fewer extreme observations with which to fit the distribution or calibrate the model. Second, we are very often forced to extrapolate well beyond the time frame of the observations (i.e., predicting the 100-yr storm with only 50 yr of rainfall data). This is especially critical when attempting to estimate a quantity such as the PMP, for which the risk of exceedence is theoretically nil. Multifractals allow us to infer the statistical properties of precipitation fields over well-defined ranges of scale from the statistical properties at the measurement timescale, including extreme events

(Schertzer and Lovejoy 1992; Lovejoy and Schertzer 1995).

Previously, Hubert et al. (1993) presented a multifractal approach for estimating the PMP, an approach that attempts to link the physical processes that generate precipitation events to the conceptual model of multiplicative cascades, and allows the PMP estimation problem to be cast in a probabilistic framework. Following Hubert et al. (1993), whenever there is a maximum singularity,  $\gamma_{\max}$ , within a duration  $\tau$ , the maximum accumulation,  $A_\lambda$ , within that duration will be

$$A_\lambda = \frac{\varepsilon_\lambda T}{\lambda} \propto \lambda^{\gamma_{\max}-1} \propto \tau^{1-\gamma_{\max}}. \quad (5)$$

Even if the singularity is theoretically unbounded, the maximum order of singularity in a finite sample will always be bounded due to spurious scaling artifacts resulting from undersampling. Thus, in applying Eq. (5), it is implicit that we are predicting the maximum event for a finite (albeit very long) time series. Furthermore, following Lovejoy and Schertzer (1995), physically observable multifractals belong to the class of universal multifractals, and thus, the actual physics that give rise to  $\gamma_{\max}$  are not relevant per se. Therefore, the multifractal representation captures the statistical properties of the observations independently of when or how extreme precipitation came to be. Universal multifractals are convenient because only two parameters,  $\alpha$  and  $C_1$ , need to be estimated:

$$c(\gamma) = \begin{cases} C_1 \left( \frac{\gamma}{C_1 \alpha'} + \frac{1}{\alpha} \right)^{\alpha'} & \text{for } \alpha \neq 1 \quad \text{and} \\ C_1 \exp \left( \frac{\gamma}{C_1} - 1 \right) & \text{for } \alpha = 1, \end{cases} \quad (6)$$

where  $1/\alpha' + 1/\alpha = 1$ . Here  $C_1$  is the codimension of the mean process  $- \{C_1 = C[K(q = 1)]\} \leq 1$  for a time series, and measures the sparseness of the data;  $\alpha$  is the Levy index, which ranges between 0 and 2 and indicates how strongly the process deviates from monofractal behavior (i.e., for simple scaling  $\alpha = 0$ ) by specifying to which type of process the probability distribution belongs (Olsson et al. 1993). For  $0 \leq \alpha < 1$  and considering a time series of infinite length, a finite maximum order of singularity,  $\gamma_0$ , can be determined as follows:

$$\gamma_0 = \frac{C_1}{1 - \alpha} \quad (7)$$

(Schertzer and Lovejoy 1992; Hubert et al. 1993). When analyzing geophysical measurements, we are always limited by the fact that we must use time series of finite length to characterize the multifractal behavior. In that case, the observed singularities will be bounded by an effective maximum singularity,  $\gamma_s$ :

$$\gamma_s = \gamma_0 \left[ 1 - \alpha \left( \frac{C_1}{D} \right)^{-1/\alpha'} \right] < \gamma_0, \quad (8)$$

where  $D$  is the embedding space dimension ( $D = 1$  in the analysis of the time series). The total dimension of this problem is actually  $(D + D_s)$ , where  $D_s = \log N_s / \log \lambda$  is the sampling dimension, and  $N_s$  is the number of independent time series at each location. ([Here  $N_s = 1$  and  $D_s = 0$ ].) In the case of “soft” multifractals ( $0 < \alpha < 1$ , such as rainfall), if  $\gamma_0 \geq \gamma_s D$  and  $\gamma_0 <$ , then the maximum effective singularity (reachable maximum event based on the observations) has a codimension that varies linearly with  $K(q)$  for  $q > q_D$  as follows [Eq. (9) replaces Eq. (6)]:

$$c(\gamma) = q_D \gamma - K(q_D) \quad \text{for } \gamma_D \leq \gamma \leq \gamma_s, \quad (9)$$

where  $q_D$  and  $\gamma_D$  are the critical orders of moments and singularities, respectively (Schertzer and Lovejoy 1992). This corresponds to a transition to self-organized criticality for  $\gamma \geq \gamma_D$  (“conditionally soft” multifractals) characterized by scale invariance, divergence of higher-order statistical moments, and falloff of the tail of the probability distribution (Schertzer and Lovejoy 1992; Schertzer et al. 1997). In the context of the theory of universal multifractals,  $q_D$  should be a universal constant characteristic of rainfall processes. There is however no clear agreement in the literature as to what such a value should be. Variations between 1.7 up to 5 have been attributed to differences in rainfall intensity and rainfall physics, orography, temporal resolution of the observations, and length of the time series (e.g., Olsson 1995; Purdy et al. 2001). Nevertheless, common values range from slightly below 2 to a little above 3. In this paper, the number of time series analyzed exceeds previous work by two to three orders of magnitude, albeit with coarser temporal resolution (1 day versus minutes or hours). We find values of  $q_D = 2 \pm 0.2$ , thus in the expected range. This will be discussed further in section 3c.

#### e. Purpose and objectives of this study

Because deficiencies in PMP estimates result in similar deficiencies in PMF determination, Dawdy and Lettenmaier (1987) suggested a risk-based approach to hydraulic design criteria. The final recommendation on this issue made by the National Research Council (NRC 1994, p. 21) was that “strategies be investigated for estimating the probabilities of extreme rainfalls, using the best available concepts and methods of meteorology and statistics.” To that end, we describe an alternative approach to PMP estimation by investigating the applicability of multifractals for estimating extreme precipitation events for the eastern United States. We call these estimates the fractal maximum precipitation (FMP) and they represent maximum events empirically derived using the scaling behavior of the observations. This method yields parameters for estimating both the magnitude and risk of extreme events, essential criteria in engineering design and decision making. That is, for a desired exceedence probability ( $p_e$ ), it is possible to

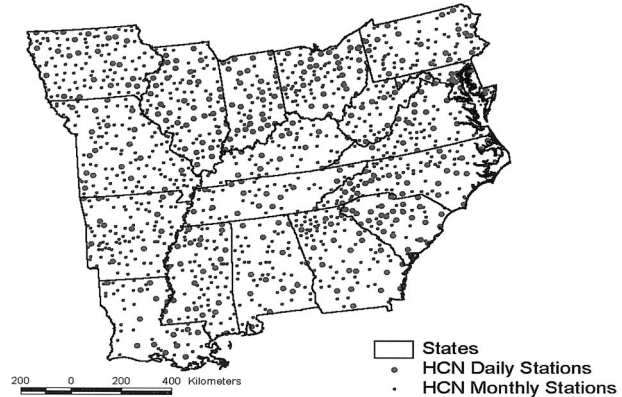


FIG. 1. Region of analysis and locations of HCN daily and monthly stations.

infer from Eq. (3) the corresponding value of the codimension  $c(\gamma_e)$ , which can then be used to estimate the magnitude of an event with the specified risk. In addition, we evaluate the effects of terrain and interdecadal climate variability on precipitation statistics, and thus multifractal parameters, and compare maximum precipitation estimates from the multifractal approach to those used in standard practice.

## 2. Methodology

### a. Precipitation data

We evaluated the scaling behavior of precipitation in the midwestern and southeastern United States using 327 daily and 1400 monthly time series from the U.S. Historical Climate Network (HCN; Karl et al. 1990). Within this region, there are 349 daily and over 3000 monthly HCN stations; however, many of the time series are short or discontinuous. For the sake of a consistent analysis, we did not use all HCN sites nor did we use the entire record at selected sites. Instead, we evaluated precipitation data collected between 1950 and 1997, a time frame that maximized both the spatial density and temporal continuity of the time series in the region of interest. The analysis domain and the locations of the daily and monthly stations used in this study are shown in Fig. 1. When an entire month was missing in a daily or monthly time series, it was filled with average values calculated from the same months in the preceding and following years, preserving the interannual variability as much as possible. Individual missing days in the daily time series were filled with the time series average. Values for 29 February were ignored. Scaling breaks were identified by evaluating maximum normalized accumulations and statistical moments over durations ranging from 1 day to 20 yr. Sample codimensions,  $c(\gamma_s)$  (hereafter simply called codimensions), were computed as the scaling slope of the maximum normalized accumulations between the scaling breaks. The interval

over which  $c(\gamma_s)$  was calculated is denoted in brackets ([ ]).

*b. Scaling parameter estimation*

Early studies recommended using the time series averages to nondimensionalize (normalize) the time series so that they represented points along a line. Lovejoy and Schertzer (1995) later reported that codimension estimation is sensitive to the normalization method, and recommended that the ensemble mean be used to normalize all time series in the analysis. So that the normalization of the time series would not confound the interpretation of our spatial and temporal comparisons, we used the regional mean computed from all time series in this study to normalize (nondimensionalize) the data. To compute codimensions, we first linearize Eq. (5) by applying a logarithmic transformation as follows:

$$\begin{aligned} \log(A_\lambda) &= B + (1 - \gamma_{\max}) \log(\tau) \\ &= B + c(\gamma_s) \log(\tau), \end{aligned} \tag{10}$$

where  $A_\lambda$  now represents the time series maximum normalized accumulation for each different resolution (duration)  $\tau$  and the term  $(1 - \gamma_{\max})$  represents the slope [or codimension  $c(\gamma_s)$ ] for  $A_\lambda$  between scaling breaks. For instance, for  $\tau = 1$ , the  $A_\lambda$  is the maximum observed normalized daily (monthly) rainfall amount taken from a daily (monthly) time series. For  $\tau = 2$ , moving 2-day (month) sums are computed and  $A_\lambda$  represents the maximum normalized 2-day (month) sum. This was done for  $\tau$  ranging from the highest resolution (1 day or 1 month) to the lowest resolution (summation over the entire time series). The codimension  $c(\gamma_s)$  and the intercept  $B$  were computed from the slope of a plot of  $\log(A_\lambda)$  versus  $\log(\tau)$  using linear regression. Then,  $\gamma_{\max}$  was computed as  $1 - c(\gamma_s)$ . We interpolated  $c(\gamma_s)$  values spatially across the entire study region using bilinear interpolation of the station values. For consistency, spatial fields could also be generated using fractal disaggregation techniques to capture small-scale variability and orographic effects (Bindlish and Barros 1996; Kim and Barros 2002). However, that type of analysis requires careful evaluation of spatial scaling properties, which is outside of the scope of this study.

*c. Multifractal parameter estimation*

To estimate the multifractal parameters  $\alpha$  and  $C_1$ , we used the double trace moment technique used by Lavallee et al. (1991), Tessier et al. (1993), and Olsson (1995), and the modified DTM technique presented by Veneziano and Furcolo (1999). A double trace moment is defined in Lovejoy and Schertzer (1995) as

$$Tr_\lambda(\varepsilon_\lambda^\eta)^q = \left\langle \sum_i \left( \int_{B_{\lambda,i}} \varepsilon_\lambda^\eta d^Dx \right)^q \right\rangle \propto \lambda^{K(q,\eta) - (q-1)D}. \tag{11}$$

As originally presented, this method entails raising the field of interest  $\varepsilon$  at its highest resolution  $\Lambda$  to various powers of  $\eta$ . In our case,  $(\int_{B_{\lambda,i}} \varepsilon_\lambda d^Dx)$  represents the precipitation intensity field ( $\varepsilon$ ) integrated over the scale of interest ( $B_{\lambda,i}$ ) in the embedding space  $D$  ( $D = 1$  for time series). For simplicity, this will be represented as  $\varepsilon_\lambda^\eta$ . For each value of  $\eta$ ,  $\varepsilon_\lambda^\eta$  is degraded to lower resolutions of  $\lambda$  by averaging over increasing durations, for example, daily precipitation time series are degraded by averaging over  $\lambda = 2, 3$ , and 4 days, and so on. The degraded field  $(\varepsilon_\lambda^\eta)_\lambda$  is then raised to a fixed power  $q$  and the  $q$ th-order moment  $\langle (\varepsilon_\lambda^\eta)_\lambda^q \rangle$  is obtained numerically by averaging the field. The moment scaling exponent  $K(q, \eta)$  is related to  $K(q)$ , [ $K(q) = K(q, 1)$ ], by

$$K(q, \eta) = \eta^\alpha K(q), \tag{12}$$

so  $\alpha$  is computed as the slope of a log-log plot of  $K(q, \eta)/K(q)$  versus  $\eta$ . A value for  $C_1$  is determined by rearranging

$$K(q) = \begin{cases} \frac{C_1(q^\alpha - q)}{\alpha - 1} & \text{for } \alpha \neq 1 \text{ or} \\ C_1 q \log(q) & \text{for } \alpha = 1 \end{cases} \tag{13}$$

from Schertzer and Lovejoy (1992). The effective theoretical maximum  $\gamma_s$  and its codimension  $c(\gamma_s)$  are then computed from Eq. (8) and Eq. (6), respectively [ $c(\gamma_s) = D + D_s = 1$  in our study as previously noted; Hubert et al. (1993)].

According to Veneziano and Furcolo (1999), the DTM method as originally presented yields unbiased  $\alpha$  estimates only for “bare” quantities (i.e., the geophysical fields at their characteristic timescale, not that of the observations). Consequently, estimates of  $\alpha$  from “dressed” quantities (observations of the field averaged over a finite sampling area) are biased when the original method is used. Veneziano and Furcolo proposed a modified DTM method for application to dressed fields by reversing the first two steps:  $\varepsilon_\lambda$  is first degraded to a lower resolution by averaging and then the lower-resolution result  $(\varepsilon_\lambda)_\lambda$  is raised to the power  $\eta$  and divided by the expected value of  $(\varepsilon_\lambda)_\lambda^\eta$ , or  $(\varepsilon_\lambda)_\lambda^\eta / \langle (\varepsilon_\lambda)_\lambda^\eta \rangle$ , where  $\langle \rangle$  denotes the average over the degraded time series. We applied both versions of the DTM and found only small differences in  $\alpha$  and  $C_1$  and essentially no difference in the final estimation of  $\gamma_0$  (see discussion in section 3).

*d. FMP and DPMP estimation*

To estimate the magnitude of the FMP magnitude, we used the slope and intercept from the regression model for the parameters  $B$  and  $c(\gamma_s)$ , respectively, in Eq. (10). Subsequently, the inverse logarithm of Eq. (10) gives

$$\text{FMP} = 10^B \lambda^{c(\gamma_s)}. \tag{14a}$$

Return periods for the FMP estimates were computed as  $1/p$  where  $p$  (the exceedence probability associated

with the FMP estimate) was obtained by substituting  $c(\gamma_s)$  into Eq. (3). The discontinuity of the moment scaling function at  $q = q_D$  indicates a change in scaling regime reflecting an increasing contribution of extreme events to the magnitude of higher-order moments. Consequently, the DPMP of the desired return period can be inferred by replacing the scaling parameter in Eq. (14a) by  $c(e)$ , where  $e > D$ :

$$\text{DPMP} = 10^B \times \lambda^{c(\gamma_e)}. \quad (14b)$$

For comparison with our analysis of precipitation data, we also computed codimensions estimates from monthly and 6-hourly precipitable water data. Precipitable water data were obtained from the (National Centers for Environmental Prediction–National Center for Atmospheric Research) reanalysis dataset. NCEP–NCAR precipitable water data are vertically averaged instantaneous values currently available at a  $2.5^\circ \times 2.5^\circ$  spatial resolution. Precipitable water fluxes were estimated by assuming that the characteristic residence time of the atmospheric column over a grid cell is determined by the characteristic speed of major storm systems (roughly  $40 \text{ mi h}^{-1}$ , or  $62 \text{ km h}^{-1}$ ). The spatial resolution of these is very coarse, but the recently completed NCEP–NCAR reanalysis (R2) data were not available during this study (Kanamitsu et al. 2002). Precipitable water parameters were estimated in the same manner as precipitation.

### 3. Results and discussion

#### a. Scaling behavior of daily and monthly precipitation time series

Major temporal scaling breaks were found to occur at 30 days (1 month) and 365 days (1 yr) as illustrated in Fig. 2, which shows the daily and monthly scaling behavior of three representative time series. For the daily data, scaling breaks for durations of less than 10 days were found to vary from station to station (also seen in Fig. 2). Consequently, the variability of estimated codimension values was greatest for durations between 1 and 10 days. However, for durations greater than 10 days, all time series exhibited similar scaling behavior with small variations around the regional ensemble mean. For the daily data, codimensions were calculated for short durations [(1–3) days, (1–4) days, (1–8) days] as well as (1–30) days. The codimensions for durations in this range were very similar in magnitude, but the (1–30) day codimension values were less variable; hence, they are deemed most appropriate for our analysis. Codimension values ranged from 0.01 to 0.49 for (1–30) day (daily) and 0.32 to 0.82 for (1–12) month (monthly; Fig. 3). These codimensions are of interest in estimating the FMP and for understanding the effects of terrain and climate variability on daily to annual extreme precipitation events as will be explored in section 3c.

#### b. Multifractal parameters and FMP estimates from daily precipitation time series

Before applying the DTM, the value of the critical moment,  $q_D$ , was evaluated in two ways: by investigating the upper tail behavior of the empirical probability density function (pdf) of the time series in log–log space (as in Olsson 1995) and by determining the point at which the relationship between  $K(q)$  and  $q$  becomes linear. Olsson (1995) reported a range of  $q_D$  for rainfall time series of  $\approx 1.7$ – $3.0$ . Figures 4a and 4b show the empirical pdf and  $K(q)$  function for an example time series from our study. Figure 4a indicates a complex tail behavior with two linear slopes, 2.1 and 3.3, determined by linear regression. Two distinct slopes, and thus two phase transitions, were evident only in time series with maxima greater than approximately 20 cm ( $8 \text{ in.}$ )  $\text{day}^{-1}$  [similar complex tail behavior was also noted in Fraedrich and Larnder (1993)]. Other less extreme time series had only one linear slope similar to Olsson (1995, Fig. 1). Linearity in the example  $K(q)$  function (Fig. 4b) occurred at approximately  $q = 2$  with a second break in slope evident at approximately  $q = 3.4$  (corresponding to the slope of 3.3 in Fig. 4a). These breaks are subtle and easier to detect when plotted in log–log space instead of linear space. By evaluating selected time series in this manner, we determined that the first phase transition occurred on average at  $q = 2 \pm 0.2$ , and thus  $q_D = 2.0$  was generally appropriate for the time series in our study.

The modified DTM technique (Veneziano and Furcolo 1999) with a fixed  $q = q_D = 2$  was used to estimate multifractal parameters  $\alpha$  and  $C_1$ . The moment exponents,  $K(2, \eta)$  were estimated using linear regression on trace moments computed for  $\tau = 1$ – $30$  days ( $\lambda = 584$ – $17\,520$ ) and  $\eta$  from 0.5 to 2.5. Figure 5 shows the range of multifractal parameter estimates obtained from the analysis of the time period between 1950 and 1997. Here,  $\gamma_s$  is within the range of observed  $\gamma_{\max}$ , but the distribution of  $\gamma_{\max}$  is wider presumably due to heterogeneous sampling. Theoretically,  $c(\gamma_s) = 1 + D_s$  and it should be  $c(\gamma_s) = 1$  in our case (Hubert et al. 1993). The median value of  $c(\gamma_s)$  was 1.0, with a range of 0.9889–1.0066 in our analysis, essentially identical to what was expected theoretically. The small amount of variation about the median was attributed to sampling variability. Additionally, we computed multifractal parameters for  $q$  ranging from 1.1 to 5 and found that parameter estimates varied only slightly between the original and the modified DTM as shown in Fig. 6. This was not surprising since our estimates of  $\alpha$  and  $C_1$  were in the range of low or no bias in the graphs presented by Veneziano and Furcolo (1999). Nevertheless, values of  $\gamma_s$  obtained from the modified DTM, while exhibiting a wider range (see Fig. 6), were much closer to the range of computed values of  $\gamma_{\max}$ , indicating that the modified DTM yielded more consistent parameter estimates for our application. This analysis also showed us that chang-

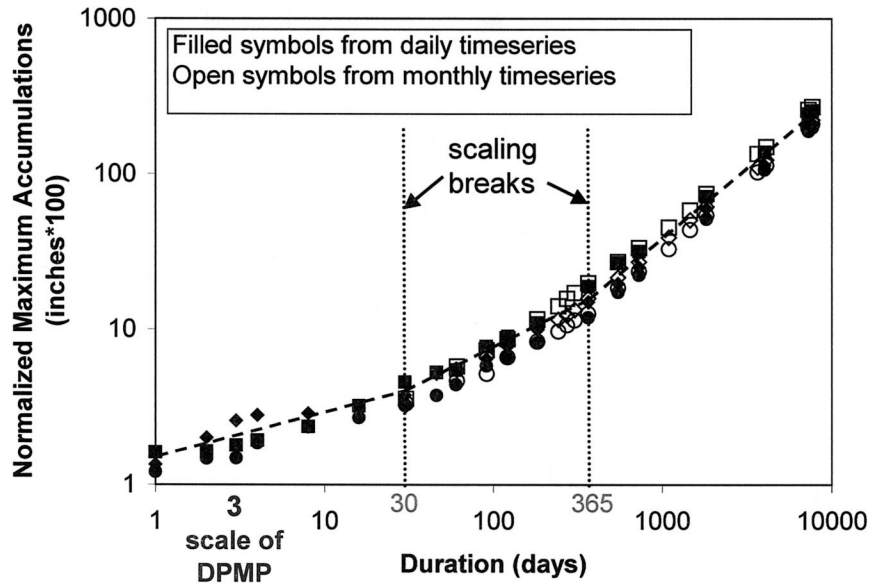


FIG. 2. Normalized maximum accumulations for three HCN daily (filled symbols) and monthly (open symbols) time series showing temporal scaling breaks at 30 days (1 month) and 365 days (1 yr). The three different shapes (diamond, square or circle) represent the three different time series.

es in parameter estimates were negligible for values of  $q$  between roughly 1.8 and 2.5, supporting our choice of  $q_D = 2$  for FMP parameter estimation.

Figure 7a shows contour maps of 3-day FMP estimates using the multifractal parameters from Fig. 5. The contours were developed from a bilinear interpolation of the FMP values estimated at daily HCN stations. Higher FMP values are associated with southern coastal areas, which is consistent with the climatology of major storm tracks in the region. The return periods for the 3-day FMP estimates range from 5300 to 6200 yr based on Eq. (3). These estimates are one order of magnitude lower than the return periods estimated by NRC (1994) and Koutsoyiannis (1999) for the 1-day PMP. In this work, we were not able to estimate the magnitude of

the 1-day FMP; in order to do so we would have needed hourly precipitation data, the analysis of which was outside of the scope of this paper. DPMP estimates for a specified return period of 1 million yr are shown in Fig. 7b.

For illustrative purposes, we compared multifractal FMP and DPMP estimates (this study), and state-of-the-practice estimates (HMRs 51 and 52) by the Federal Energy Regulatory Commission for seven dam locations in Pennsylvania (Table 1). The HMRs 51 and 52 estimates were corrected with an orographic factor that accounted for elevation and wind direction. The DPMP map for Pennsylvania in Fig. 8, also showing dam locations, was enlarged from Fig. 7b. Ratios of multifractal FMP estimates to HMRs 51 and 52 estimates in Table 1 range from 0.50 to 1.04, with five of the seven ratios between 0.50 and 0.66. The implications of this example are twofold. First, the comparison suggests that, as expected, FMP estimates are lower than PMP estimates. The rather large difference may be due to the relatively short time series used in our analysis. Second, it stresses the importance of incorporating spatial variability and terrain in the analysis. On the other hand, the DPMP estimates are consistently higher than the standard PMP (DPMP/PMP ratios ranged from 0.96 to 2), suggesting that they can be used as a bound of known risk in design of critical infrastructure.

The multifractal method presented in this study shows promise as an alternative method for estimating the magnitude of a design event and its associated failure risk for high-hazard structures. On a cautionary note, FMP estimates are only as good as the observational record,

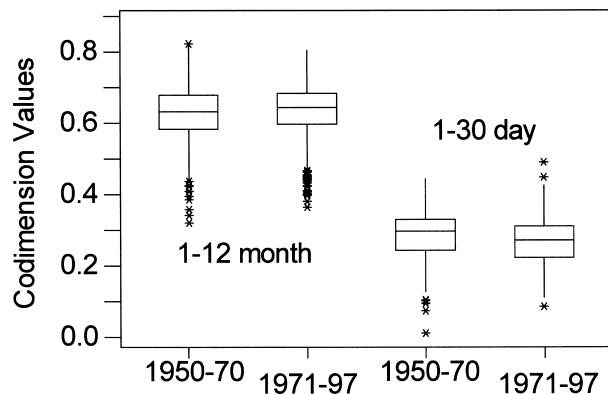


FIG. 3. Distribution of codimension values of interest computed from daily [(1-30) day codimensions] and monthly [(1-12) month codimensions] time series.



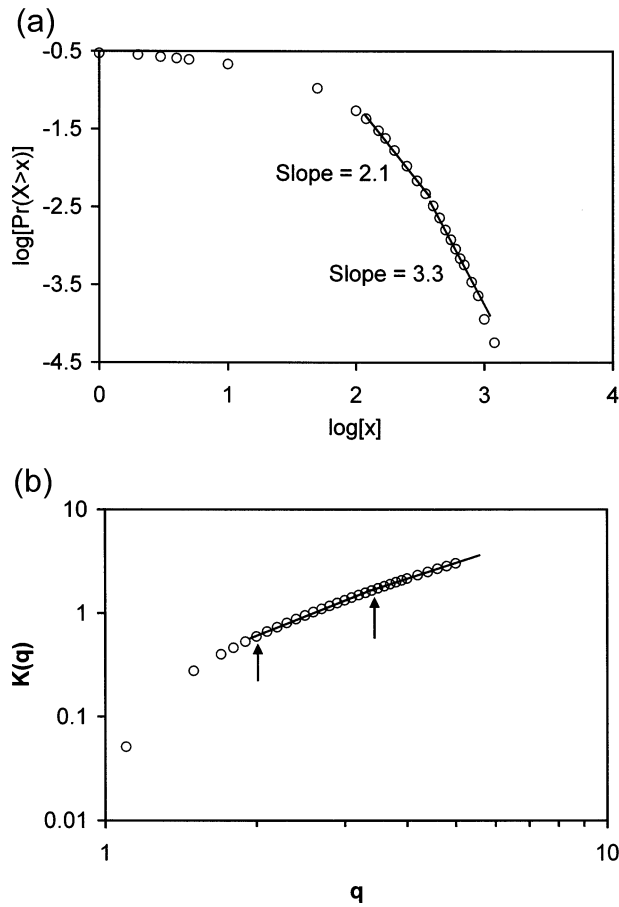


FIG. 4. (a) Example empirical pdf analysis (following Olsson 1995) for determining  $q_D$  in our study. Note the complex tail behavior (two linear slopes) that was evident only in time series with maxima greater than 20 cm (8 in.) day<sup>-1</sup>. (b) Example  $K(q)$  function for the same time series as in (a). The point at which linearity occurred ( $q = 2$ ) was more easily discerned when the function was plotted in log-log space. Note the subtle break in slope that corresponds to the second slope in (a).

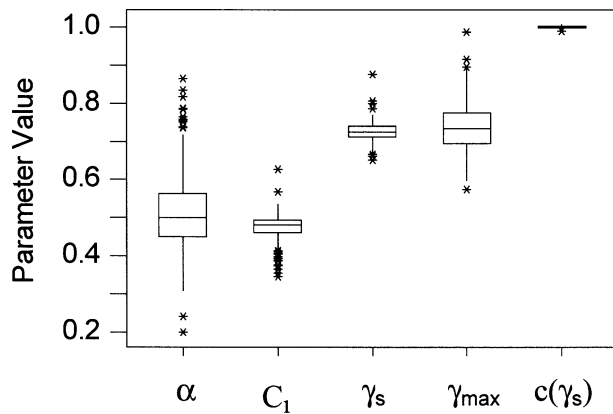


FIG. 5. Multifractal parameters estimated from daily HCN time series for 1950–97.

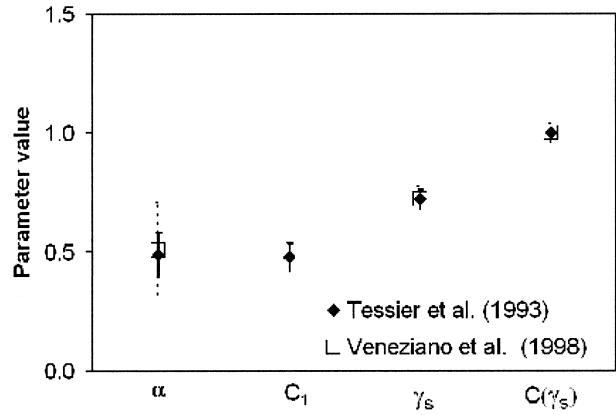


FIG. 6. Comparison of multifractal parameters obtained by applying the original DTM method (as presented in Tessier et al. 1993) and the modified method presented by Veneziano and Furcolo (1999).

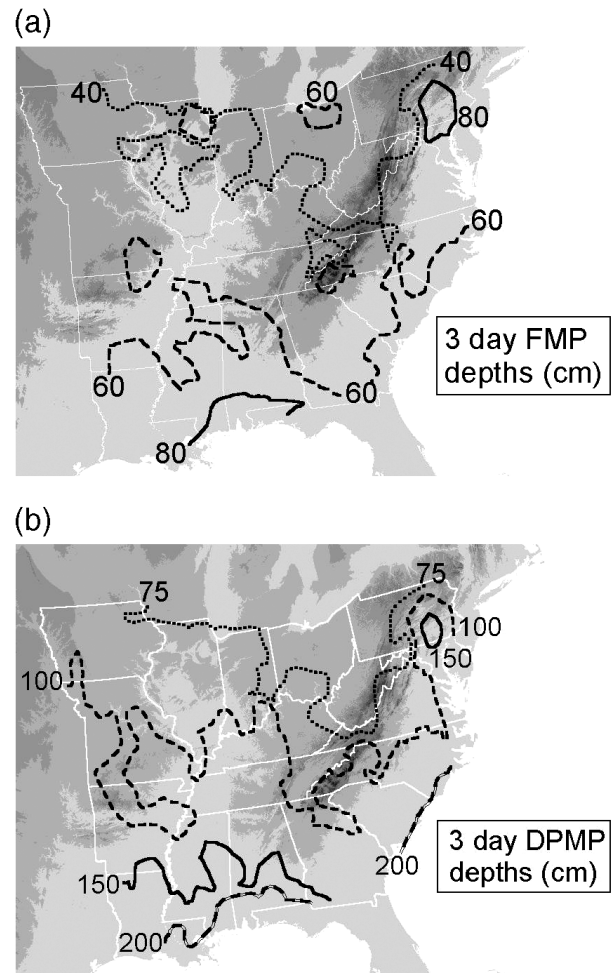


FIG. 7. (a) The 3-day FMP depth contours (in cm) estimated using parameter estimates shown in Fig. 5. (b) The 3-day DPMP depth contours (in cm) estimated using parameter estimates shown in Fig. 5.

TABLE 1. Comparison of FMP and DPMP estimated using methods presented in this paper with PMP estimates using HMRs 51 and 52 (NWS 1980a; Hansen et al. 1982) with orographic correction. See Fig. 8 for dam site locations.

Dam site	HMRs 51 and 52 PMP (cm)	FMP (cm)	DPMP (cm) for $P_e = 1 \times 10^{-6}$	Ratio of FMP/PMP	Ratio of DPMP/PMP
7	72.03	36.58	70	0.51	0.97
4	77.22	38.85	74	0.50	0.96
11	65.02	67.53	130	1.04	2.00
25	65.02	59.98	115	0.92	1.77
20	68.07	44.75	86	0.66	1.26
16	68.07	44.75	86	0.66	1.26
2	68.07	43.12	83	0.63	1.22

which requires long-term monitoring at high spatial resolution. It must also be recognized and accepted that using the FMP as a design criterion would likely expose the structure and those dependent on the safety of the structure to a higher degree of failure risk than that designed using the conventional PMP, or alternatively the DPMP as defined here.

*c. Effect of climate variability and terrain on FMP parameters and estimates*

To investigate whether there is an effect of interdecadal climatic variability on the values of multifractal parameters, each time series was split into two subseries (1950–70 and 1971–97). For the daily [(1–30) day] codimensions, the mean decreased from 0.285 to 0.269, but this change was not statistically significant. We found that daily codimensions along the Atlantic and Gulf coasts decreased over time, which coincided with increased daily precipitation maxima in the later period. For the monthly codimensions, the mean value increased from 0.629 to 0.637 between the two time frames, a change that is statistically significant at a 95% confidence level. The combined effects of terrain and climate were investigated by grouping the daily and monthly codimensions from the two time frames (1950–70 and 1971–97) into four elevation categories as a function of rain gauge elevation: 1) <61 m (200 ft), 2) 61–244 m (200–800 ft), 3) 244–427 m (800–1400 ft), and 4) >427 m (1400 ft). These elevation categories roughly coincide with relevant physiographic regions: 1) relatively flat coastal plains and broad river valleys, 2) gently sloping plateau (analogous to first upslopes defined in section 1), 3) steeply sloping foothills (analogous to secondary upslopes as defined in section 1), and 4) mountain ridges. The average (1–30) day and (1–12) month codimensions and the corresponding 95% confidence intervals in the four terrain categories are shown in Figs. 9a and 9b, respectively. In general, the differences in daily codimension fields from one time period to another are stronger than the spatial variations for the same period. For example, (1–30) day codimension distributions have similar ranges across the elevation categories, but all

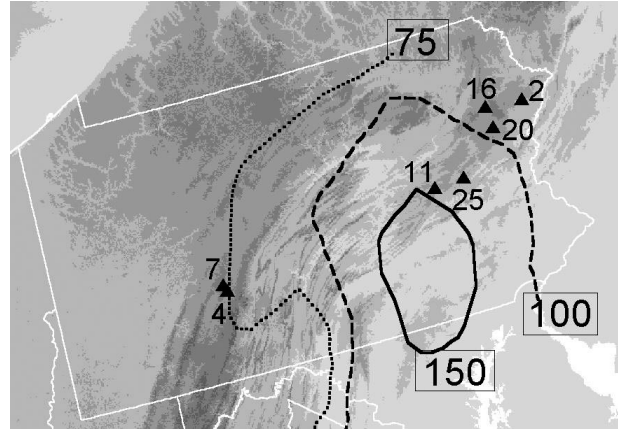


FIG. 8. Dam site locations (triangles) overlaid on 3-day DPMP contour map over PA (enlarged from Fig. 7b). Comparisons of PMP estimated using HMRs 51 and 52 with FMP and DPMP (this paper) are given in Table 1.

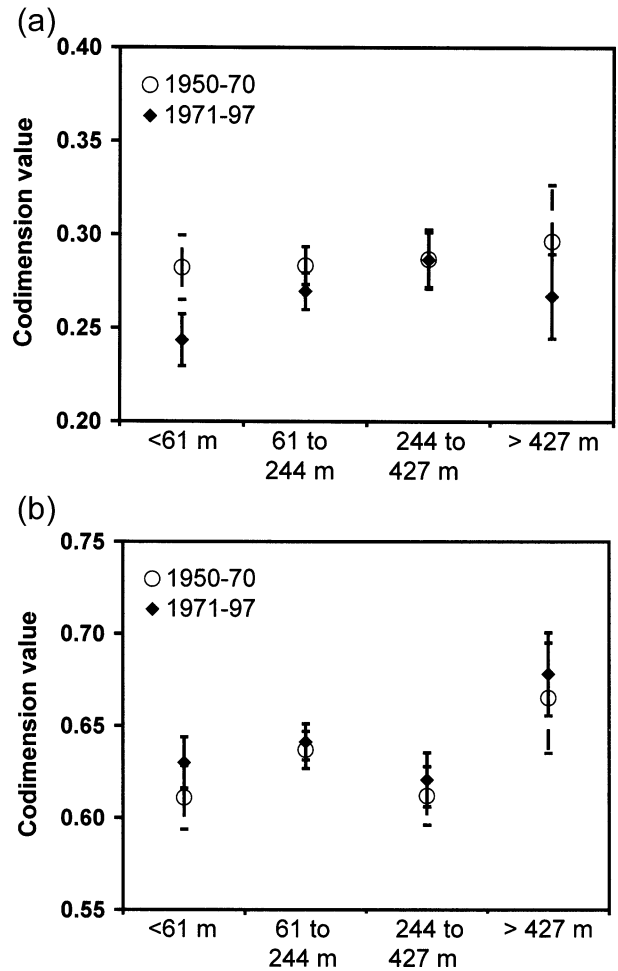


FIG. 9. (a) Mean values with 95% confidence intervals for (1–30) day codimensions showing the influence of both climate variability and terrain. (b) Mean values with 95% confidence intervals for (1–12) month codimensions showing the influence of both climate variability and terrain.

show a slight downward shift from the earlier to the later time frame. In the lowest-elevation category (coastal plains and river valleys) the mean daily codimension values for the two time periods are significantly different at a 95% confidence level (Fig. 9a). This indicates that daily rainfall has become more extreme in the coastal areas. For the (1–12) month codimension, interdecadal variability has not had a large influence on the mean codimensions or their distribution, but terrain has. Changes in monthly codimensions are indicative of changes at the seasonal to annual scales (an increased (1–12) month codimension signifies an upward trend in annual total precipitation). Orographic enhancement of annual total precipitation is evident in Fig. 9b in that the average codimension values for the highest-elevation category ( $>427$  m) are statistically higher than the other categories. Although a rigorous spatial analysis was not performed, this evaluation suggests that at long timescales (i.e., monthly to yearly), spatial variations in rainfall accumulations primarily are congruent with orography and landform, while at short timescales (i.e., daily) the same variations reflect variations in weather statistics likely associated with interdecadal climatic variability. Nevertheless, note that scaling analysis implicitly requires stationarity of the time series. By splitting the observational record into two periods, we effectively hypothesize that this is not the case. Further research toward determining the record length necessary to accommodate both stationarity and sampling requirements is needed.

#### d. Scaling behavior of precipitable water

By definition, the underlying assumption in estimating the PMP is that the maximum amount of atmospheric moisture falls as precipitation. To illustrate the relationship between heavy rainfall and atmospheric water, we studied the scaling behavior of 6-hourly fields of precipitable water fluxes from the NCEP–NCAR reanalysis datasets. Contours of maximum 6-h precipitable water (PWAT) fluxes for 1950–97 are shown in Fig. 10. The shallower column of atmosphere over which the atmospheric moisture is integrated to compute precipitable water is evident in the tongue of lower flux values over the Appalachian Mountains. Also evident are the higher PWAT fluxes over the Gulf of Mexico and the tropical Atlantic, both areas that serve as sources of atmospheric moisture. For comparison, we highlight the location of severe flash flooding in West Virginia, which occurred in response to very intense storm activity on 2 May 2002. The highest (preliminary) recorded rainfall amount (13 cm or 5.1 in.) was in Elkhorn, West Virginia; however, it was reported that more than 4 in. of the rain fell within a 6-h period. This accumulation corresponds to about half of the maximum PWAT flux estimated in the vicinity. Preliminary data from the three closest rain gauges surrounding Elkhorn are significantly lower on the same day: Athens (HCN-

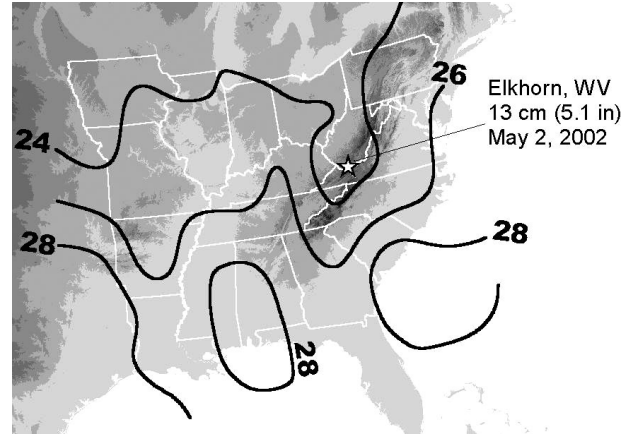


FIG. 10. Maximum 6-h precipitable water flux contours (in cm) for 1950–97. The four counties in WV that experienced severe flash flooding in early May 2002 are highlighted. Elkhorn, WV, recorded the highest (preliminary) daily precipitation accumulation on 2 May 2002, 13 cm (5.1 in.), most of which was reported to have fallen within a 6-h period.

460355) recorded 6.91 cm (2.72 in.), Bluefield (HCN-460925) recorded 6.99 cm (2.75 in.), and Princeton (HCN-467207) recorded 7.11 cm (2.80 in.). This case clearly illustrates the large space–time variability of rainfall, which challenges the reliability of regionalized estimates of hydrological extremes when the spatial resolution of the observing network cannot capture small-scale, heavy storms such as thunderstorms, localized orographic convection, etc.

To place the FMP estimates from the previous section within the framework of total available atmospheric moisture for the same time period, we repeated our analysis for the 6-h PWAT time series. Scaling breaks were identified at 30 days, 6 months, and 12 months. A subtle but important scaling break was also identified at 3 days. Discrete Fourier transform (DFT) analysis showed that the characteristic frequency in the PWAT time series was 5 days, which is consistent with the interarrival times of large storm systems. Because precipitable water columns are moving (whereas the ground-based precipitation depth measurements were not), using a time interval greater than 3–5 days to compute multifractal PWAT parameters ( $\alpha$ ,  $C_1$ ,  $\gamma_s$ , etc.) would not be valid. We found that only the codimensions obtained from the  $[6 \text{ h } 3 \text{ day}^{-1}]$  duration yielded the required  $\alpha < 1$  (with the exception of one outlier), which is the limit of validity for Eq. (7). With the exception of the (6–12) month codimensions, all other codimensions were close to the embedded scale dimension (D) of 1 (the embedding dimension can be thought of as representing the “space filling” properties of rainfall accumulations). Inspection of their spatial codimension distributions (not shown) illustrated that interdecadal climate variability effects are pronounced in a manner consistent with our findings with regard to the codimensions of observed precipitation maxima.

#### 4. Conclusions

In this study we characterized the multifractal behavior of maximum accumulated daily and monthly precipitation time series and maximum accumulated 6-h precipitable water fluxes for the period from 1950 to 1997. We chose this relatively short time frame because it maximized the number of suitable time series within our analysis domain. We evaluated a multifractal approach for estimating high-hazard engineering design criteria. The multifractal method also provides a framework to assign a risk of exceedence for the PMP. Return periods for the 3-day FMP estimates in this study ranged from 5300 to 6200 yr, an order of magnitude lower than previous estimates for the standard PMP. We computed FMP magnitudes for illustrative comparison with PMP estimates from the conventional NWS approach (HMRs 51 and 52) that had been corrected for orographic effects. For selected dam sites in Pennsylvania, 3-day multifractal FMP estimates were typically 50%–70% of the PMP 3-day estimates. The size of this underestimation may be due in part to the relatively short time frame used in this analysis. Nevertheless, note that occasionally the FMP/PMP ratio is close to or exceeds unity. This underscores the importance of site-specific, place-based estimates of extreme events. By contrast, multifractal estimates of extreme events with a return period of 1 million yr generally exceed the standard HMRs 51 and 52 PMP values and, thus, can be viewed as an upper bound of known risk to the PMP. For design purposes, the entire time series should be used in order to obtain the most conservative DPMP estimates. Further theoretical work is needed to investigate the introduction of historical maxima into empirical multifractal analysis, when the historical record is broken or incomplete.

We also investigated the effects of climate variability and terrain and found that codimensions (timescaling slopes) calculated over short durations [i.e., (1–30) days] capture changes in weather associated with interdecadal climatic variability, while spatial patterns in these codimensions are reflective of synoptic weather patterns and moisture sources. Codimensions calculated over longer durations [i.e., (1–12) months] are more influenced by terrain and less by climate variability. Since FMP estimates are calculated for relatively short durations, typically ranging from 6 h to 3 days, we conclude that FMP estimates are subject to the same influences as the daily codimensions from which these estimates are derived. We also found that the scaling behavior of precipitable water fields from the NCEP–NCAR reanalysis was similar to that of precipitation from rain gauge observations in that the spatial patterns of codimensions at short timescales were more reflective of synoptic weather patterns, while spatial patterns for seasonal to interannual timescales reflected regional physiography, namely the dominant presence of the Appalachian Mountains.

Although the multifractal method shows promise for

yielding physically meaningful design criteria, this work suggests that any estimates based on rain gauge observations will always be constrained by the length of the record and by the spatial resolution of the rain gauge network. Further research should be conducted to investigate how robust the relationship is between the scaling of model-simulated precipitable water fluxes and observed rainfall. As the spatial and temporal resolution of numerical weather prediction models improves, long-term climate simulations may provide an avenue to gather data for using in risk-based estimates of extreme rainfall.

*Acknowledgments.* This work was first presented at the 2002 Spring Meeting of the American Geophysical Union, Washington D.C. This work was inspired after Hubert et al. (1993). The research was supported in part by the National Aeronautics and Space Administration under Grant NAG5-7547 with the second author. Dr. Timothy Lang provided support during the analysis of the NCAR data. The authors wish to thank D. Koutsoyannis and G. Bonin for their useful comments and suggestions.

#### REFERENCES

- Barros, A. P., and D. P. Lettenmaier, 1994: Dynamic modeling of orographically-induced precipitation. *Rev. Geophys.*, **32**, 265–284.
- , and R. J. Kuligowski, 1998: Orographic effects during a severe wintertime rainstorm in the Appalachian Mountains. *Mon. Wea. Rev.*, **126**, 2648–2671.
- Bindlish, R., and A. P. Barros, 1996: Aggregation of digital terrain data using a modified fractal interpolation scheme. *Comput. Geosci.*, **22**, 907–917.
- Collier, C. G., and P. J. Hardaker, 1996: Estimating probable maximum precipitation using a storm model approach. *J. Hydrol.*, **183**, 277–306.
- Dawdy, D. R., and D. P. Lettenmaier, 1987: Initiative for risk-based flood design. *J. Hydraul. Eng.*, **113**, 1041–1051.
- Foufoula-Georgiou, E., 1989: A probabilistic storm transposition approach for estimating exceedence probabilities of extreme precipitation depths. *Water Resour. Res.*, **25**, 799–815.
- Fraedrich, K., and C. Larnder, 1993: Scaling regimes of rainfall time series. *Tellus*, **45A**, 289–298.
- Frisch, U., and G. Parisi, 1985: Fully developed turbulence and intermittency. *Turbulence and Predictability in Geophysical Fluid Dynamics and Climate Dynamics*, M. Ghil et al., Eds., North-Holland, 84–88.
- Graham, W. J., 2000: Should dams be modified for the probable maximum flood? *J. Amer. Water Resour. Assoc.*, **36**, 953–963.
- Gupta, V. K., and E. Waymire, 1990: Multiscaling properties of spatial rainfall and river flow distributions. *J. Geophys. Res.*, **95** (D3), 1999–2009.
- Halsey, T. C., M. H. Jensen, L. P. Kadanoff, I. Procaccia, and B. I. Shaiman, 1986: Fractal measures and their singularities. *Phys. Rev. A*, **33**, 1141–1151.
- Hansen, E. M., L. C. Schreiner, and J. F. Miller, 1982: Application of probable maximum precipitation estimates, United States east of the 105th meridian. Hydrometeorological Rep. 52, National Weather Service, Silver Spring, MD, 176 pp.
- Hershfield, D. M., 1961: Estimating the probable maximum precipitation. *J. Hydraul. Div., Amer. Soc. Civ. Eng.*, **87**, 99–106.
- , 1965: Method for estimating probable maximum precipitation. *J. Amer. Water Works Assoc.*, **57**, 965–972.

- Hubert, P., and Coauthors, 1993: Multifractals and extreme rainfall events. *Geophys. Lett.*, **20**, 931–934.
- Kanamitsu, M., W. Ebisuzaki, J. Woollen, S. K. Yang, J. J. Hnilo, M. Fiorino, and G. L. Potter, 2002: NCEP–DOE AMIP-II reanalysis (R-2). *Bull. Amer. Meteor. Soc.*, **83**, 1631–1643.
- Karl, T. R., C. N. Williams Jr., F. T. Quinlan, and T. A. Boden, 1990: United States Historical Climatology Network (HCN) serial temperature and precipitation data. Environmental Science Division Publ. 3404, Carbon Dioxide Information and Analysis Center, Oak Ridge National Laboratory, Oak Ridge, TN, 389 pp.
- Kim, G., and A. P. Barros, 2002: Downscaling of remotely-sensed soil moisture with a modified fractal interpolation method using contraction mapping and ancillary data. *Remote Sens. Environ.*, **83**, 400–413.
- Koutsoyiannis, D., 1999: A probabilistic view of Hershfield's method for estimating probable maximum precipitation. *Water Resour. Res.*, **35**, 1313–1322.
- Lavallee, D., D. Schertzer, and S. Lovejoy, 1991: On the determination of the codimension function. *Non-linear Variability in Geophysics*, D. Schertzer and S. Lovejoy, Eds., Kluwer Academic, 99–109.
- Lovejoy, S., and D. Schertzer, 1985: Generalized scale invariance in the atmosphere and fractal models of rain. *Water Resour. Res.*, **21**, 1233–1250.
- , and —, 1990: Multifractals, universality classes and satellite and radar measurements of cloud and rain fields. *J. Geophys. Res.*, **95** (D3), 2021–2034.
- , and —, 1995: Multifractals and rain. *New Uncertainty Concepts in Hydrology and Water Resources*, Z. W. Kundzewicz, Ed., International Hydrology Series, Cambridge University Press, 336 pp.
- , —, and J. D. Stanway, 2001: Direct evidence of multifractal atmospheric cascades from planetary scales down to 1 km. *Phys. Rev. Lett.*, **86**, 5200–5203.
- Meneveau, C., and K. R. Sreenivasan, 1987: Simple multifractal cascade model for fully developed turbulence. *Phys. Rev. Lett.*, **59**, 1424–1427.
- NRC, 1994: *Estimating Bounds on Extreme Precipitation Events*. National Academy Press, 29 pp.
- NWS, 1980a: Probable maximum precipitation estimates, United States east of the 105th meridian. Hydrometeorological Rep. 51, Silver Spring, MD, 92 pp.
- , 1980b: Seasonal variation of 10-mile-square probable maximum precipitation estimates, United States east of the 105th meridian. Hydrometeorological Rep. 53, Silver Spring, MD, 94 pp.
- , 1982: Application of probable maximum precipitation estimates—United States east of the 105th meridian. Hydrometeorological Rep. 52, Silver Spring, MD, 176 pp.
- , 1983: Probable maximum precipitation and snowmelt criteria for southeast Alaska. Hydrometeorological Rep. 54, Silver Spring, MD, 124 pp.
- , 1984: Probable maximum precipitation estimates, Colorado River basin and Great Basin drainages. Hydrometeorological Rep. 49, Silver Spring, MD, 169 pp.
- , 1986: Probable maximum and TVA estimates of precipitation with areal distribution for Tennessee River drainages less than 3,000 mi<sup>2</sup> in area. Hydrometeorological Rep. 56, Silver Spring, MD, 241 pp.
- , 1988: Probable maximum precipitation estimates, United States between the Continental Divide and the 103rd meridian. Hydrometeorological Rep. 55A, Silver Spring, MD, 259 pp.
- , 1994: Probable maximum precipitation—Pacific Northwest states, Columbia River (including parts of Canada), Snake River and Pacific coastal drainages. Hydrometeorological Rep. 57, Silver Spring, MD, 347 pp.
- , 1999: Probable maximum precipitation for California. Hydrometeorological Rep. 59, Silver Spring, MD, 395 pp.
- Olsson, J., 1995: Limits and characteristics of the multifractal behavior of a high-resolution rainfall time series. *Nonlinear Processes Geophys.*, **2**, 23–29.
- , J. Niemczynowicz, and R. Berndtsson, 1993: Fractal analysis of high-resolution rainfall time series. *J. Geophys. Res.*, **98** (D12), 23 265–23 274.
- Purdy, J. C., D. Harris, G. L. Austin, A. W. Seed, and W. Gray, 2001: A case study of orographic rainfall processes incorporating multiscaling characterization techniques. *J. Geophys. Res.*, **106** (D8), 7837–7845.
- Schertzer, D., and S. Lovejoy, 1987: Physical modeling and analysis of rain and clouds by anisotropic scaling of multiplicative processes. *J. Geophys. Res.*, **92D**, 9693–9714.
- , and —, 1992: Hard and soft multifractals. *Physica A*, **185**, 187–194.
- , —, F. Schmitt, Y. Chigirinskaya, and D. Marsan, 1997: Multifractal cascade dynamics and turbulent intermittency. *Fractals*, **5**, 427–471.
- Svensson, C., and P. R. Rakhecha, 1998: Estimation of probable maximum precipitation for dams in the Hongru River catchment, China. *Theor. Appl. Climatol.*, **59**, 79–91.
- Tessier, Y., S. Lovejoy, and D. Schertzer, 1993: Universal multifractals: Theory and observations for rain and clouds. *J. Appl. Meteor.*, **32**, 223–250.
- , —, P. Hubert, D. Schertzer, and S. Pecknold, 1996: Multifractal analysis and modeling of rainfall and river flows and scaling, causal transfer functions. *J. Geophys. Res.*, **101** (D21), 26 427–26 440.
- Veneziano, D., and P. Furcolo, 1999: A modified double trace moment method of multifractal analysis. *Fractals*, **7**, 181–195.
- Wang, B.-H. M., 1984: Estimation of probable maximum precipitation: Case studies. *J. Hydraul. Eng.*, **110**, 1457–1472.

Copyright of Journal of Hydrometeorology is the property of American Meteorological Society and its content may not be copied or emailed to multiple sites or posted to a listserv without the copyright holder's express written permission. However, users may print, download, or email articles for individual use.